Comparison of Spectroscopic and Probe data in a Magnetic Mirror Helium Plasma

S. Knott, C. Roche, A.A. Ruth, P.J. McCarthy

Physics Department, University College Cork, Ireland

1. Introduction

A Helium plasma discharge is initiated in a magnetic mirror through thermionic emission from a coiled tungsten wire, of diameter 0.5 mm and total length 20 cm, located ≈ 3-4 cm above the centre point of the mirror, negatively biased with respect to the walls of the vessel. The magnetic mirror is formed using a pair of NdFeB rare earth magnets of length 20 cm and diameter 3 cm mounted in contact with the surface of a cylindrical water-cooled vacuum vessel (see Figure 1), with $B_{max} \approx$ 0.5 T on the inside wall of the vessel and $B_{min} \approx 5$ mT at the centre of the mirror. Using a Langmuir Spatial Probe system of Impedans Ltd., data is acquired at 5 mm intervals spanning a 300 mm range. The full probe characteristic for mirror plasmas can be accurately fitted with an in-house data analysis program which assumes a bi-Maxwellian [1] (primary (thermionic) and secondary (ionisation) electrons) electron energy distribution, necessary to model the significant primary/hot electron population that is confined by the mirror - a consequence of the filament's location within the mirror. An Ocean Optics dispersion spectrometer with wavelength range $220\,\text{nm} < \lambda < 800\,\text{nm}$ is used to acquire the spectroscopic data which is taken via the use of a vernier scale fibre holder that allows the acquisition of a fan of sight-lines. An inversion is then performed to find the 2D emissivity function for each He I line. This is evaluated along the trajectory of the movable probe system, thus allowing comparison between local emissivities and local density and temperature determined from Langmuir probe analysis. Determination of Electron Density n_e and Temperature T_e by spectroscopic means is a candidate diagnostic in the divertor leg of the MAST Upgrade Tokamak due to its passive, non-intrusive nature.

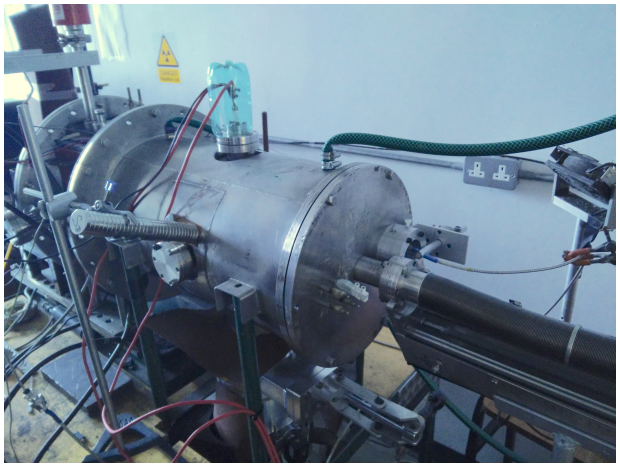

Figure 1: Image of Cylindrical vessel (25x45 cm), movable axial probe, Spectral window and Magnet stack

2. Inversion model

The inversion model used is based on Zernike polynomials, which were chosen for their property of orthogonality on the unit disk, and take the form:

$$Z_n^m(\rho,\theta) = R_n^m(\rho)\cos(m\theta) \qquad (1)$$
$$Z_n^{-m}(\rho,\theta) = R_n^m(\rho)\sin(m\theta)$$

[1] model includes a small contribution from the re-emitted wall electrons. [7]

where the radial polynomials R_n^m are defined as:

$$R_n^m(\rho) = \begin{cases} \sum_{k=0}^{\frac{n-m}{2}} \frac{(-1)^k (n-k)!}{k!(\frac{n+m}{2}-k)!(\frac{n-k}{2}-k)!} \rho^{n-2k} & \text{n-m even} \\ 0 & \text{n-m odd} \end{cases} \tag{2}$$

where ρ is the distance from the centre of the vessel, while θ is the angle with respect to the horizontal vessel axis. The first 15 Zernike Polynomials were used corresponding to n and m ranging from $0 \rightarrow 4$. For radial distances greater than the mirror axis-filament separation, Langmuir data analysis shows the electron density falls off exponentially with an attenuation length of approximately 4 cm. To take account of this observed behaviour, the Zernike polynomials were combined with an exponential attenuation factor to take into account the fall off of intensity within the vessel as the electron density decreases. In addition, terms were included to take into account the size of the vessel and the finite size of the acceptance angle of the fibre.

3. Probe characteristic fitting model

We use the original orbit motion limited (OML) Mott-Smith-Langmuir model [1], combined with the recently discovered importance of charge exchange (CX) reactions for the ion current [2], to fit the overall probe current i_p as a function of the bias voltage V. The model for the probe current i_p is now described:

$$i_p = i_{e,c} + i_{e,h} + i_{e,w} + i_{ion} \tag{3}$$

where $i_{e,c/h}$ is the contribution from cold/hot electron populations while $i_{e,w}$ is the weak contribution from the wall population included in the model [7]. Let $\eta = (V - V_p)/T_e$ where V_p is the plasma potential and T_e is the cold, hot or wall electron temperature expressed in electron volts and let $i_{e,0} = n_e e\, \bar{v}_e A_p/4$ be the species current at $V = V_p$ where $\bar{v}_e = \sqrt{8eT_e/(\pi m_e)}$. Then

$$\frac{i_e}{i_{e,0}} = \begin{cases} e^{\eta}\,; & V < V_p \\ s(1 - \mathrm{Erfc}\sqrt{\frac{\eta}{s^2-1}}) + e^{\eta}\mathrm{Erfc}\sqrt{\frac{\eta}{1-s^{-2}}}\,; & V > V_p \end{cases} \tag{4}$$

where $s = 1 + x_s/a_p$ is the sheath radius normalized to the probe radius a_p, and x_s is the sheath thickness. The sheath model is as described in [2]

The ion current $i_{ion} = i_{i,OML} + i_{i,CX}$ is modelled as a sum of OML and CX contributions. The roles of the electron retarding ($V < V_p$) and accelerating ($V > V_p$) expressions in eq. (4) are reversed for ions, and the accelerating expression for $V < V_p$ can be shown [2] to simplify to

$$i_{i,OML} = \frac{n_0 e\, A_p \sqrt{2}}{\pi} \sqrt{\frac{-e(V - V_p)}{M}} \tag{5}$$

where M is the ion mass. The CX contribution is calculated from (see [2], eq. 21)

$$i_{i,CX} = 2\pi n_0 n_n e\, \ell \int_{a_p}^{s} \sqrt{\hat{V}}\, \sigma_{CX}(\hat{V})\, r\, dr \tag{6}$$

where $\hat{V} = -2e(V - V_p)/M$, n_n is the neutral density, ℓ the probe length and the $\mathrm{He}{-}\mathrm{He}^+$ CX cross-section is given by [4] $\sigma_{CX} = 27.9 \times 10^{-20}(1 - 0.0557 \ln E)^2$ m^2 where the ion energy E is in units of eV.

4 Results

Given the homogeneous helium pressure, and hence target population for excitation, we would expect the emissivity to be approximately proportional to the hot electron density, as the cold electron temperature, being far weaker than the helium excitation energy will make a comparatively negligible contribution to the emissivity. Figure 2 shows results derived from Langmuir probe and spectroscopic data acquired from a plasma with the following parameters: helium pressure (P) = 3 mTorr, plasma current = 3.5 A, filament bias voltage (V_d) = 60 V, heating circuit voltage (V_{fil}) = 44 V and total heating power = 1.1 kW.The Langmuir probe density data shown in figure 2 (a), demonstrates a clear off-axis peak located at approximately 7 cm. This is due to the location of the filament (above the centre point) within the mirror leading to an azimuthal drift of the emitted primary electrons giving a strong asymmetry in the probe data with only one side being shown to allow comparison with the dominant side of the recovered emissivity distribution. The Temperature data from the Langmuir probe, figure 2 (b), shows a drop in the hot temperature from approximately 60 eV to 30 eV as the probe retracts from the centre of the vessel. This is due to the hot electrons losing energy due to ionisation and excitation of the neutral helium.

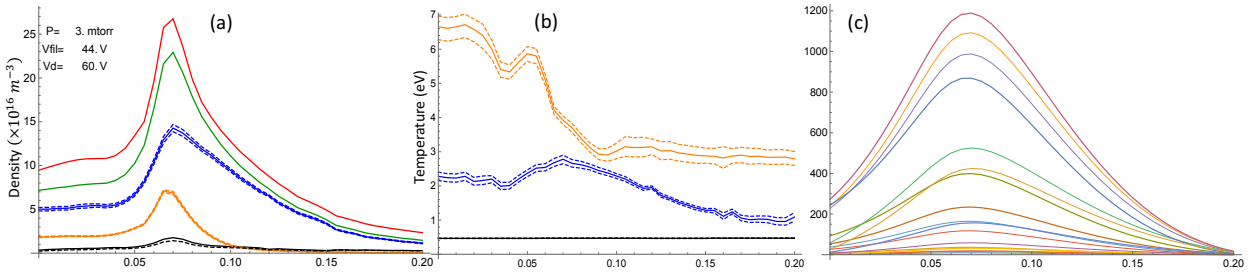

Figure 2: (a) The density for the **Cold**, **Hot**, and **Wall**, electrons along with their **sum**, and the $n_e \propto I^2$, electron density against radial distance ρ, (b) The **Cold**, **0.1×Hot**, and **Wall** Temperature vs radial distance ρ and (c) Intensity of all 17 He I lines plotted against radial distance ρ.

The inversion process was carried out for each of 17 prominent He I lines. These 17 lines are shown together in figure 2 (c) and separated for clearer reading in figure 3. All lines show an off centre peak located at approximately 7 cm from the centre of the vessel. This off axis intensity peak agrees with the location of the peak density in Figure 2 (a).

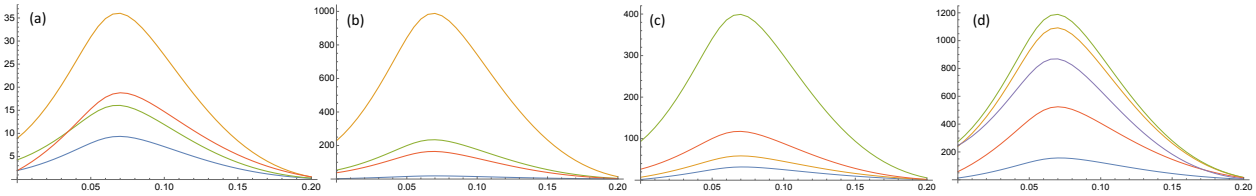

Figure 3: Intensities of 17 He I lines evaluated along the $\theta = 0^o$ axis from 2-D emissivity distributions reconstructed from measured line-integrated spectra, where (a) **318**, **361**, **370** and **381** nm lines (b) **388**, **396**, **402** and **411** nm lines (c) **438**, **446**, **470** and **491** nm lines (d) **501**, **587**, **667**, **706** and **728** nm lines

Due to uncertainties about the validity of the 2D inversion process (as shown in Figure 4) due to the single fan of sightlines, a more robust if cruder option is to consider the raw data directly. Figure 2 (a) shows that, beyond the peak location at $\rho \approx 7$ cm, the density decays strongly with distance from the centre of the vessel, i.e. the magnetic mirror axis. This allows the external sightlines to be used as a proxy for the density with the low angles viewing the centre of the plasma (and hence

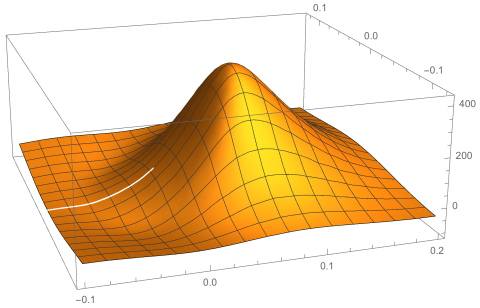

Figure 4: Example of the 2D emissivity reconstruction, shown here for the 728 nm line

a high density region) as well as the outer regions while the high viewing angles would only capture the low density remote regions of the mirror. Line ratios shown in figure 5 demonstrate the effect of the density on different combinations of line ratios, as the viewing angle is swept from the remote portions of the plasma to the central core. In figure 5 (a) and (d) the line ratio increases as the viewing angle changes showing the denser and hotter core of the mirror, while the opposite is true for the line ratio in figure 5 (b). Some lines such as that shown in figure 5 (c) show no dependence on the viewing angle, and therefore on the plasma parameters, meaning that both lines (587 and 402 nm) have the same dependency on the density and temperature of the electrons.

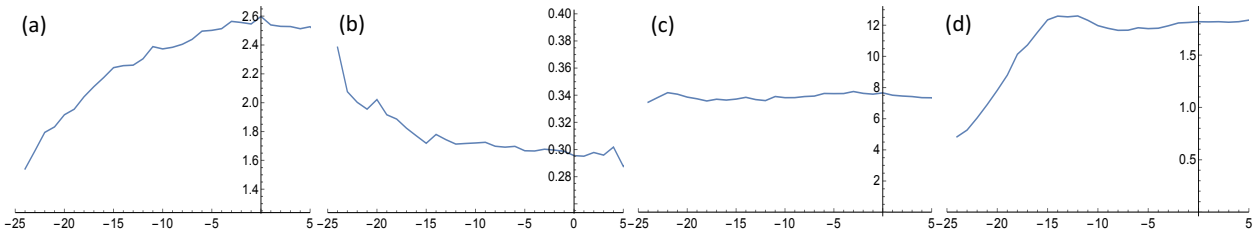

Figure 5: Line Ratios against external viewing angle whith each graph showing the following ratio (all in nm) (a) $\frac{447}{402}$ (b) $\frac{471}{447}$ (c) $\frac{587}{402}$ (d) $\frac{447}{396}$

5 Summary and Outlook

That density and emissivity peaks occur at the same radial position indicates the viability of the inversion process. Figure 5 demonstrates the viability of the line ratio method as a diagnostic for the determination of n_e and T_e, as do the multiple line crossings in figure 2 (c). Alternative mirror geometries are being planned with the goal of an axisymmetric emissivity distribution with a central peak which will simplify the modelling. New diagnostic windows, allowing for additional fans of sightlines are also under consideration.

References

[1] H. M. Mott-Smith, I. Langmuir, Phys.Rev. **28** (1926) 727.
[2] Z. Sternovsky, S. Robertson, M. Lampe, Phys. Plas. **10** (2003) 300.
[3] V.A. Godyak, V.P. Meytlis, H.R. Strauss, IEEE Trans. Plas. Sc. **23** (1995) 728.
[4] S.A. Maiorov, Plas. Phys. Rep. **35** (2009) 802.
[5] A.R. Field, P.G. Carolan, N.J. Conway, M.G. O'Mullane, Rev. Sci. Instr. **70** (1999) 355.
[6] S. Lisgo et al., J. Nucl. Mat. **390-91** (2009) 1078.
[7] S. Robertson,Z. Sternovsky, Physical Review E 72, 016402 (2005)

This work has been carried out within the framework of the EUROfusion Consortium and has received funding from the Euratom research and training programme 2014-2018 under grant agreement No 633053. The views and opinions expressed herein do not necessarily reflect those of the European Commission.